Phenomenological Lifetime Assessment for Turbine Housings of Turbochargers

F. Laengler[1], T. Mao[2], H. Aleksanoglu[2] and A. Scholz[2]

[1]BorgWarner Turbo Systems Engineering GmbH, Marnheimer Strasse 85/87, D-67292 Kirchheimbolanden, Germany; Email: FLaengler@borgwarner.com
[2]Institut fuer Werkstoffkunde, Technische Universitaet Darmstadt, Grafenstrasse 2, D-64283 Darmstadt, Germany; Email: Scholz@mpa-ifw.tu-darmstadt.de

ABSTRACT. *The turbine housing of a turbocharger is exposed to extensive cyclic thermo-mechanical loading. This leads to multi-axial stress states with local plastifications, so that the design of the turbine housing becomes a major challenge in ensuring the guaranteed lifetime in relation to the high-temperature behavior of the materials. The first step was to develop and validate a phenomenological lifetime estimation approach, in conjunction with a constitutive material model applied in a preceding Finite-Element analysis, for application on the casting materials Ni-resist D5S and GJV. A satisfactory estimation of the number of cycles until crack initiation, by considering creep fatigue interaction, was demonstrated on specimens subject to characteristic load conditions derived by a critical plane approach. In the second step, the adaption for turbine housing design is investigated.*

INTRODUCTION

An important key component of a turbocharger is the turbine housing (T/H) that provides the kinetic energy required for charging. Inhomogeneous temperature distributions and the interaction with neighboring components constrain the thermal expansion and contraction of the T/H, thus causing local multi-axial stresses and inelastic strains during operation. The combination of thermal transients with mechanical load cycles leads to thermo-mechanical fatigue (TMF) and, ultimately, after a certain number of loading cycles, to component failure. Numerous test stand runs are generally inevitable in order to find the appropriate combination of the complex design and the material. Hence, there is a demand for reliable calculation methods allowing lifetime estimation early in the design process, for instance, to employ the full potential of materials and to reduce the effort and expense for component testing by better understanding the cyclic mechanical long term behavior at elevated temperatures. Improvements in this respect can be expected in terms of coupling the numerical component structural analysis with validated lifetime estimation approaches based on physical damage effects.

The phenomenological lifetime estimation approach presented was developed on

rules for the synthesis of stress-strain path and relaxation, wherein creep fatigue interaction is included. The lifetime calculation is proposed as a post-processing step depending on the results of a preceding Finite-Element analysis. The constitutive material model applied therein describes the elastoplastic material behavior using an associated flow rule with the MISES yield surface and a kinematic hardening law.

Validation and application of the TMF lifetime calculation until crack initiation by comparison with experimental results is performed on casting material of type Ni-resist D5S and vermicular cast iron GJV. Both thermal shock tests on turbine housings and TMF tests on specimens subject to complex change of temperature and strain have been conducted for identification and verification purposes.

COMPONENT STRUCTURAL ANALYSIS

Reliable stress and strain states as a response to cyclic thermo-mechanical loading can be numerically calculated in a component structural analysis only if the constitutive equations used are able, in particular, to describe the temperature-dependent cyclic plasticity. However, the cost-benefit ratio has to be allowed for in this case owing to the numerous different T/H materials used in passenger car and commercial diesel applications. Consequently, an acceptable effort taken in both determining required material-dependent parameters and numerical calculation of entire turbocharger models using commercial software, such as ABAQUS [1], is essential.

The adapted, constitutive material model describes the rate-independent elastoplastic material behavior while elastic strains remain infinitesimal. The incremental constitutive formulation of the material model is given in Table 1.

Table 1. Constitutive elastoplastic material model.

$$\mathrm{d}\mathbf{E} = \mathrm{d}\mathbf{E}^{\mathrm{el}} + \mathrm{d}\mathbf{E}^{\mathrm{pl}} \tag{1}$$

$$\mathbf{T} = \mathbf{D}^{\mathrm{el}} : \mathbf{E}^{\mathrm{el}} \tag{2}$$

$$\mathrm{d}\mathbf{E}^{\mathrm{pl}} = \mathrm{d}\bar{E}^{\mathrm{pl}} \frac{\partial \phi}{\partial \mathbf{T}} \ , \ \mathrm{d}\bar{E}^{\mathrm{pl}} = \sqrt{\frac{2}{3} \mathrm{d}\mathbf{E}^{\mathrm{pl}} : \mathrm{d}\mathbf{E}^{\mathrm{pl}}} \tag{3}$$

$$\phi = f - T_Y = 0 \tag{4}$$

$$f = \sqrt{\frac{3}{2} \left(\mathbf{T}^{\mathrm{dev}} - \boldsymbol{\alpha}^{\mathrm{dev}} \right) : \left(\mathbf{T}^{\mathrm{dev}} - \boldsymbol{\alpha}^{\mathrm{dev}} \right)} \tag{5}$$

$$\mathrm{d}\boldsymbol{\alpha}_k = C_k \frac{1}{T_Y} \left(\mathbf{T} - \boldsymbol{\alpha} \right) \mathrm{d}\bar{E}^{\mathrm{pl}} - \gamma_k \boldsymbol{\alpha}_k \mathrm{d}\bar{E}^{\mathrm{pl}} + \frac{1}{C_k} \boldsymbol{\alpha}_k \frac{\partial C_k}{\partial \theta} \mathrm{d}\theta \ , \ \mathrm{d}\boldsymbol{\alpha} = \sum_{k=1}^{n} \mathrm{d}\boldsymbol{\alpha}_k \tag{6}$$

The (mechanical) strain rate tensor d$\mathbf{E}$ in Eq. (1) is a linear combination of the reversible elastic part d$\mathbf{E}^{\mathrm{el}}$ and the irreversible inelastic part, which is reflected solely by

the plastic strain rate $d\mathbf{E}^{pl}$ [2]. The stress tensor $\mathbf{T}$ is determined by the elastic strain tensor $\mathbf{E}^{el}$ on the basis of the HOOKEAN law of Eq. (2). In this case, the elasticity tensor $\mathbf{D}^{el}$ of forth-order is not affected by inelastic deformation. The plastic part of the deformation is defined by the assumed associated flow rule, Eq. (3), whereby $d\bar{E}^{pl}$ represents the equivalent plastic strain rate. The pressure-independent MISES yield surface ϕ allowing for kinematic hardening is defined by Eq. (4), whereby f denotes the equivalent MISES stress with respect to the overall backstress $\boldsymbol{\alpha}$. The deviatoric part of the backstress $\boldsymbol{\alpha}^{dev}$ and the stress deviator tensor $\mathbf{T}^{dev}$ are included in the conditional Eq. (5) of f. The equivalent stress T_Y defines the size of the yield surface at zero plastic strain. The non-linear kinematic hardening model is based on the work of CHABOCHE [3],[4]. The overall backstress is composed of multiple backstress components $\boldsymbol{\alpha}_k$. The non-isothermal evolution law of the strain valued backstress component $\boldsymbol{\alpha}_k$, formulated in Eq. (6), is defined to be an additive decomposition, in which a temperature rate term ensures that the material response is independent of temperature history and, consequently, can be characterized by isothermal uniaxial work hardening data. C_k and γ_k are material parameters; C_k is the initial kinematic hardening modulus and γ_k determines the rate to which the hardening modulus is decreased with increasing plastic strain.

In terms of parameter identification, only the cyclic stabilized elastoplastic material condition, after the material hardened or softened toward a stable limit, is of interest. Isothermal, strain controlled low-cycle fatigue (LCF) tests were conducted for D5S and GJV by applying symmetric triangular shaped cycles fully reversed (R_ε=-1) without a dwell period at a constant strain rate $dE_{11}=10^{-3}s^{-1}$ on unnotched specimens (see also Figure 4). The material-dependent parameters were identified at mid-life by error minimization in a least-squares sense with the gradient-based LEVENBERG-MARQUARD algorithm [5]. This results in several datasets of best-fitted parameters, each assigned to a given temperature. In the case of anisothermal calculations, the parameter set required for a certain temperature has to be interpolated between the underlying datasets.

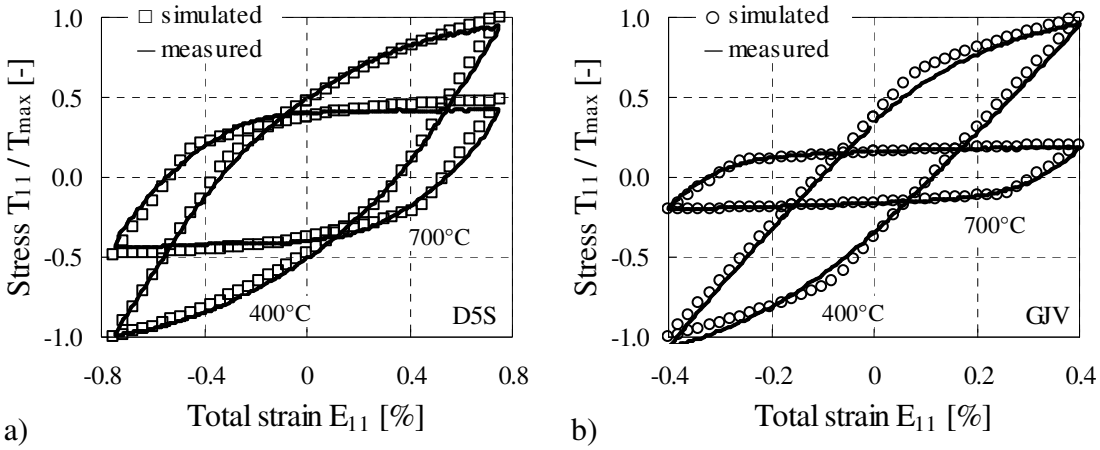

Figure 1. Measured and simulated axial stress-strain hysteresis loops from isothermal LCF tests at mid-life for a) D5S and b) GJV.

Figure 1 shows the adjustment of the constitutive elastoplastic material model to cyclic stabilized stress-strain hysteresis loops of LCF tests conducted at 400°C and 700°C with reasonable accuracy. The graphs are shown in terms of the axial strain E_{11} and the axial stress T_{11} in the LAGRANGIAN representation. The stress axis is standardized separately for each graph with the maximum stress appearing in the range of both temperatures to keep the proportions.

The introduced temperature-dependent cyclic plasticity model has proven successful in numerous applications by correlation with experimental results of thermal shock tests. The turbine housing of a regulated single stage turbocharger designed in two variants for D5S and GJV, subject to thermal shock loading, serves as the reference to assess the numerical component structural analysis. During the thermal shock test on a gas test stand, the T/Hs were removed time and time again after a certain number of load cycles for detecting crack initiations as well as monitoring crack propagations by dye penetration.

In order to simulate the corresponding thermo-mechanical T/H behavior under thermal shock test conditions by an anisothermal Finite-Element analysis on the basis of the model shown in Figure 2a for the GJV design, it is necessary to prescribe the transient temperature field as thermal boundary conditions. For this purpose, steady-state conjugate heat transfer calculations at several operation points, allowing for the interdependency of solids and fluids in heat transfer, and subsequent transient solid body temperature calculations have been performed [6].

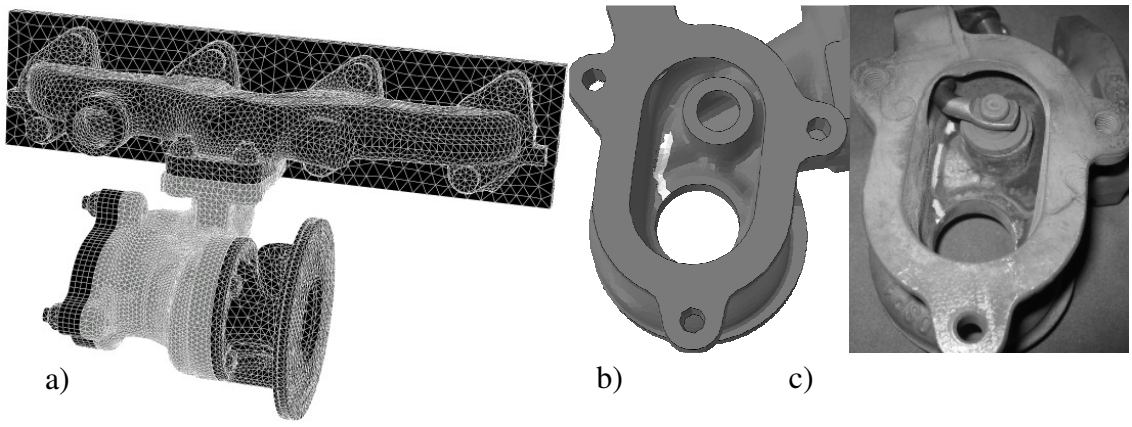

Figure 2. a) Finite-Element model for thermo-mechanical analysis of the GJV turbine housing marked gray, b) contour plot of the calculated equivalent plastic strain $\bar{E}^{pl}$ compared to c) the measured crack position on the interior wall surface of the wastegate flap valve chamber.

For example, the interior transition wall surface of the wastegate flap valve chamber downstream of the turbine volute outlet was identified as a critical position by numerical analysis in excellent agreement with experimental results, as can be seen in Figure 2b-c with the area highlighted in white. The position of increasing equivalent plastic strain $\bar{E}^{pl}$ coincides with the measured crack initiation and crack propagation, respectively.

TMF TESTING

In terms of damage evaluation to investigate the fatigue and creep fractions until crack initiation, a test series of in-phase TMF tests was performed on unnotched material specimens in a special TMF test rig shown in Figure 3a. Temperature as well as strain vs. time sequences are in accordance with Figure 3b-c.

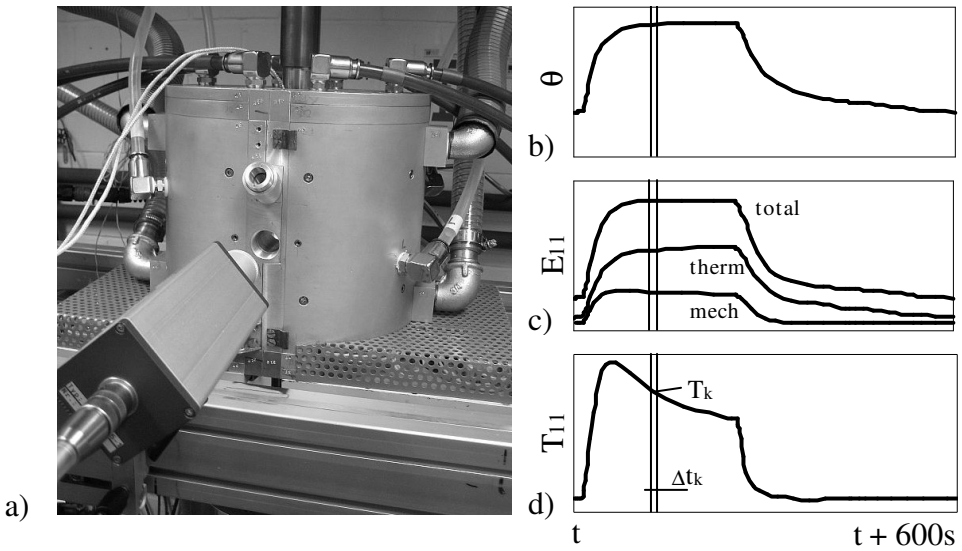

Figure 3. a) Experimental set-up for TMF testing, example of in-phase b) temperature θ and c) axial strain E_{11} load sequences inducing d) axial stress response T_{11}.

The significant TMF loading history is derived on the surface of T/H relevant critical positions as results of the Finite-Element analysis described above. During loading the principal stress directions are time-variable and multiple slip planes, which may cause fatigue damage, are activated. Thus, for each time step, the transient stress tensor **T** of multi-axial stress states is rotated into the critical plane that is defined by the maximum normal stress. The normal stress $T_{(\mathbf{n})}$ results from the dot products with the normal vector **n** of the plane considered, shown in Eq. (7). It should be characteristic for low-ductile/brittle materials such as cast iron that fatigue damage is caused primarily at the plane of maximum normal stress, see e.g. [6].

$$T_{(\mathbf{n})} = \mathbf{n}^{T} \cdot \mathbf{T} \cdot \mathbf{n} \tag{7}$$

The total normal strain $E_{(\mathbf{n})}^{\text{total}}$, decomposed in a thermal $E_{(\mathbf{n})}^{\text{therm}}$ and mechanical $E_{(\mathbf{n})}^{\text{mech}}$ component, acting on the plane of calculated maximum normal stress, is outlined as a function of time in Figure 3c. The additively superimposed thermal strain E^{therm}, given by the coefficient of thermal expansion subject to the temperature sequence θ of Figure 3b from 230°C up to above 720°C, is the same in all directions due to the assumed isotropic material properties.

The experimental life endurance results in Figure 4 are subjected to the type of

material at LCF, described by the bilinear MANSON-COFFIN relationship [8],[9], as well as under TMF loading. The values of the mechanical strain width range in axial direction ΔE_{11}^{mech} are standardized separately for each material on the maximum appearing value. Due to different strength/deformation behavior of both materials and its different creep resistance, TMF loading leads to unequal TMF lifetime behavior.

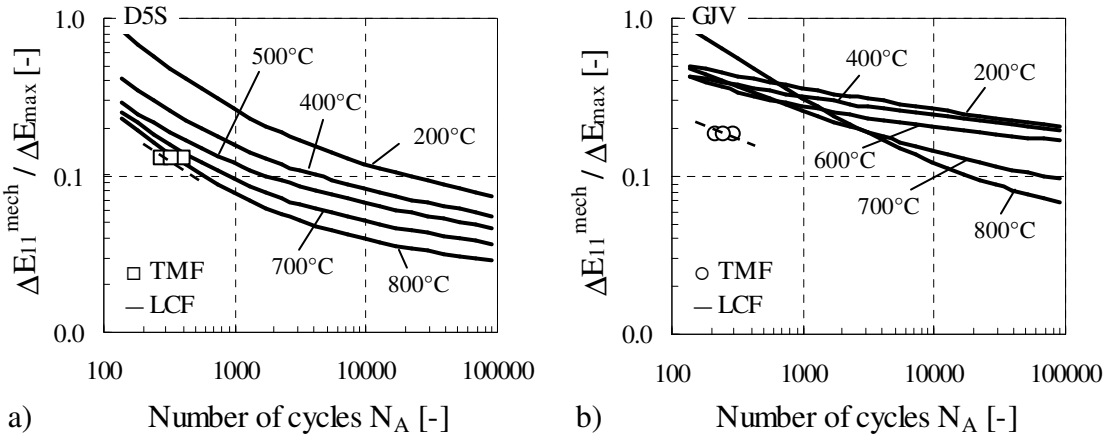

Figure 4. TMF testing results compared to LCF life curves for a) D5S and b) GJV.

PHENOMENOLOGICAL LIFETIME APPROACH

For lifetime assessment under creep fatigue loading, the life fraction rule was introduced by ROBINSON/TAIRA [10]. Failure is determined by the summation of fatigue damage L_f representing a cyclic fraction and creep damage L_c representing a time fraction summing up to the number of cycles until crack initiation N_A. The damage evaluation [11],[12] follows Eq. (8) resulting in the material-dependent creep fatigue damage L.

$$L_c + L_f = N_A \left(l_f + l_a \right) = N_A \left(\sum_k \frac{\Delta t(T_{11})_k}{t_u(T_{11})_k} + \frac{1}{N_{Ao}} \right) = L \tag{8}$$

Creep damage is calculated with respect to variation of stress during a cycle (see e.g. Figure 3b-d). At an individual increment k within a cycle and the corresponding time interval length Δt as well as axial stress T_{11}, the rupture time t_u was derived from a stress vs. time rupture curve.

$$\frac{1}{N_{Ao}} = \frac{1}{2} \left[\frac{1}{N_A \left(\Delta E_{11}^{mech}, \theta_{max} \right)} + \frac{1}{N_A \left(\Delta E_{11}^{mech}, \theta_{min} \right)} \right] \tag{9}$$

In the case of fatigue damage, it is proposed that the LCF life curves (Figure 4) at maximum cycle temperature θ_{max} and minimum cycle temperature θ_{min} be considered. In order to calculate a geometric temperature-dependent mean value of fatigue life N_{Ao} at a typical ratio $N/N_A=0.5$, that means on the cyclic stabilized material condition, the relationship shown in Eq. (9) was introduced.

Based on this phenomenological approach for lifetime estimation, the numerical calculation method developed to perform recalculation of the number of cycles until crack initiation envelopes the input of uniaxial TMF cycle and temperature-dependent material data. The procedure starts with the synthesis of temperature-dependent cyclic stress-strain (-time) behavior according to the RAMBERG-OSGOOD relationship [13] followed by the calculation of stress relaxation at relevant temperatures by means of underlying creep data. The constitutive material model as introduced above is not capable of capturing time-dependent deformation. Therefore, the relaxation is recalculated by the use of both, the NORTON-BAILEY power law [14] to describe creep strain and the strain-hardening rule [15] defining the path between creep curves related to stress changes. The determination of creep damage l_c and fatigue damage l_f, Eq. (8), both derived from the cycle at mid-life, represents cycle-dependent damage values. The estimated number of cycles until crack initiation N_{Ae} is finally determined by Eq. (10). This relationship has been derived from Eq. (8) to use the material-specific mean creep fatigue damage value L_{crit} as a critical value given, e.g., by the damage evaluation of TMF tests.

$$N_{Ae} = \frac{L_{crit}}{l_{c\,(N/N_A=0.5)} + l_{f\,(N/N_A=0.5)}} \tag{10}$$

LIFETIME ASSESSMENT

Following Eqs (8) and (9), creep damage fraction and fatigue damage fraction have been determined by use of a representative cycle at mid-life on the basis of the TMF tests conducted. This assumption is justified due to minor hardening and softening effects of the investigated materials D5S and GJV, respectively. The summation of creep damage and fatigue damage gives a mean value of the critical creep fatigue damage sum $L_{crit}=3.16$ for D5S and $L_{crit}=0.29$ for GJV.

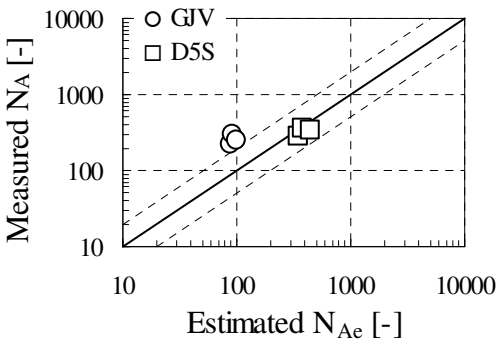

Figure 5. Recalculated number of cycles until crack initiation N_{Ae} of TMF tested specimens for D5S and GJV.

Adopting the evaluated damage sums for TMF testing recalculation of the number of cycles until crack initiation N_{Ae} provides acceptable lifetime estimation as

can be seen in Figure 5 when compared to measured values of N_A. In the case of D5S, results are relatively non-conservative, while results of GJV are significantly conservative. To reduce the conservative GJV result, the damage caused by the first load cycle has to be additionally accounted for due to the significant peak stress drop after the first cycle that is typical for lamellar and vermicular cast iron under high-temperature loading. It may be caused by the thermal-damaged graphite inclusions.

Nevertheless, applying the lifetime approach by using the preliminary evaluated critical damage sums together with the normal stress on the critical plane defined by the maximum normal stress, Eq. (7), as the stress input variable for recalculation of the number of cycles until crack initiation of the thermal-shocked T/Hs provides the results shown in Figure 6b.

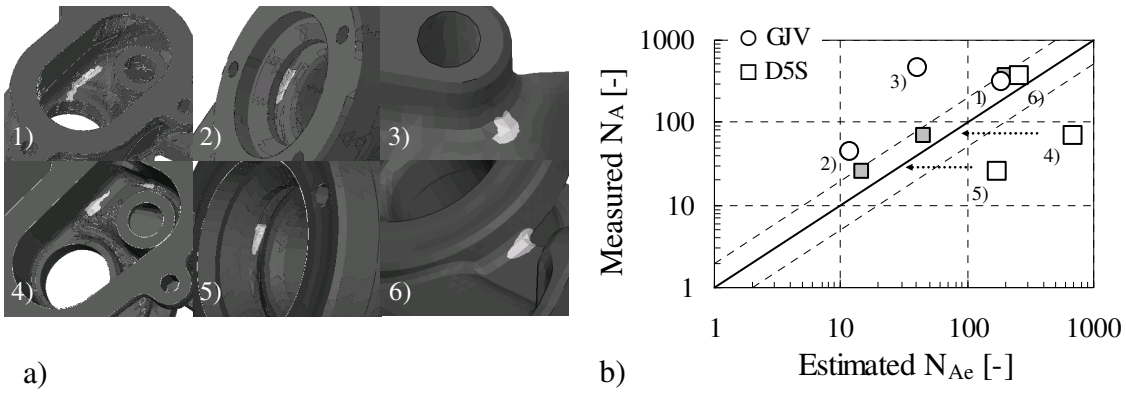

Figure 6. a) Contour plots of calculated equivalent plastic strain $\bar{E}^{pl}$ at positions of crack initiation for GJV housing 1-3 and D5S housing 4-6, respectively and b) corresponding recalculated number of cycles until crack initiation N_{Ae} compared to the averaged measured results N_A during thermal shock test.

The positions, highlighted in white, of increasing equivalent plastic strain $\bar{E}^{pl}$ calculated by the Finite Element analysis in the manner described bring out the positions of crack initiation during the thermal shock test in an excellent way (Figure 6a). For GJV the estimated numbers of cycles are significantly conservative (Figure 6b, 1-3) just as seen above in Figure 5, while for D5S the results are significantly non-conservative (Figure 6b, 4-5), except in case 6. Instead, by using the equivalent MISES stress $f_{(n)}$

$$f_{(n)} = \sqrt{T_{(n)}^2 + 3\tau_{(n)}^2} \quad , \quad \tau_{(n)} = \sqrt{\mathbf{n}^T \cdot \mathbf{T}^2 \cdot \mathbf{n} - T_{(n)}^2} \tag{11}$$

calculated with normal stress $T_{(n)}$ and shear stress $\tau_{(n)}$ on the critical plane **n** defined by maximum normal stress as the stress input variable for lifetime calculation shifts the D5S results in the conservative range, indicated with gray filled square symbols in Figure 6b. These results may denote that in the case of the more brittle GJV, material failure is dominated by normal stress. By contrast, for a better failure description of the more ductile D5S, a shear stress component has to be additionally accounted for.

CONCLUSIONS

The calculation of stress and strain based on the material model described is of adequate accuracy for numerical component structural analysis and subsequent TMF lifetime assessment as pointed out.

The lifetime estimation approach, which has been developed, demonstrates a satisfactory estimated number of cycles until crack initiation on unnotched specimens, while the adaption for T/H design is still ongoing. The scatter band of the estimated results on critical T/H positions clarifies the requirement for more experimental and analytical work to confidently improve the method. Its application comprises potential pertaining to recalculation of stress relaxation as well as the description of creep strain behavior. Hence, the systematic load analysis has led to better knowledge about acting damage mechanism, whereas an established critical damage sum is still to optimize for both materials. In addition, the analysis of microstructural phenomena should help to enhance the creep fatigue interaction together with a more detailed failure description. Actually, e.g., it is assumed that tension and compression stress have equal effect on creep and no distinction is made when calculating the creep damage. But the creep strain caused by compression stress and the resultant creep damage should be of a lower magnitude when compared to tension stress of same magnitude.
In a further step, it is proposed to describe crack propagation following the estimation of crack initiation as part of the approach. This enables expansion of the lifetime assessment up until leakage and design failure. First results on both specimens and the T/H show a clear influence.

REFERENCES

[1] Abaqus, Dassault Systèmes, 2008.
[2] Aravas, N. & E.C. Aifantis: (1991) *Int. J. Plast.* **7**: 141–160.
[3] Chaboche, J.L. (1986) *Int. J. Plast.* **2**: 149-188.
[4] Chaboche, J.L. (1989) *Int. J. Plast.* **5**: 247-302.
[5] More, J. (1977) *The Levenberg-Marquard algorithm, Implementation and Theory*, Springer, Berlin.
[6] Heuer, T., Engels, B. & P. Wollscheid (2005). In: *Proceedings of ASME Turbo Expo*, June 6-9, Reno-Tahoe, Nevada, USA.
[7] Sonsino, C.M. (2003) *Materialwissenschaft und Werkstofftechnik* **34**, 189-197.
[8] Manson, S.S. (1954) *Technical Report No. 2933*, NACA.
[9] Coffin, L. F. (1954) *Transactions of ASME* **76**, 931-950.
[10] Taira, S. (1962). In: *Structures*, pp. 96-119, N.J. Hoff (Ed.), Academic Press, New York.
[11] Scholz, A., Schmidt, A., Samir, A. & C. BERGER (2004) *Acta Metallurgica Sinica* **17**, 407-413.
[12] Scholz, A. & C. Berger (2005) *Materialwissenschaft und Werkstofftechnik* **36**, 722-730, 2005.
[13] Ramberg, W. & W.R. Osgood (1943) Technical Report No. 902, NACA.
[14] Norton, F.H. (1929) The creep of steel at high temperature, McGraw Hill, New York.
[15] Collins, J.A. (1993) Failure of materials in mechanical design: analysis, prediction, prevention, 2nd ed., Wiley & Sons, New York.